第 34 卷第 8 期
2018 年 8 月

无 机 化 学 学 报
CHINESE JOURNAL OF INORGANIC CHEMISTRY

Vol.34 No.8
1555-1565

颗粒细化过程中 Si 粉的微观结构变化对其在 KOH 水溶液中制氢性能的影响

廖 健 吴朝玲* 陈云贵 钟 爽 廖虔诚 崔立尧
(四川大学材料科学与工程学院新能源系,成都 610064)

摘要:研究了高能球磨对 Si 粉微观结构和水解制氢性能的影响。球磨过程中,颗粒尺寸不断减小,非晶转变发生,晶界、内应力、位错以及晶格变形等微观缺陷不断增加,有利于提高 Si 粉的制氢性能;但随着球磨时间的延长,颗粒团聚趋于严重,粉末氧化不断加剧,降低了 Si 粉的制氢性能。当球磨时间为 1 h,Si 粉具有最优的制氢性能,70 ℃水解时其放氢量为 1 484.2 mL·g^{-1}_{Si},但由于水解副产物 SiO_2 包覆在 Si 表面导致其转化率为 94%,无法继续完全水解。

关键词:制氢;水解;颗粒细化;Si-H_2O 反应
中图分类号:O613.72 **文献标识码**:A **文章编号**:1001-4861(2018)08-1555-11
DOI:10.11862/CJIC.2018.175

Effect on Hydrogen Generation of Microstructures of Refined Si Powders in KOH Aqueous Solution

LIAO Jian WU Chao-Ling* CHEN Yun-Gui ZHONG Shuang LIAO Qian-Cheng CUI Li-Yao
(*Department of Advanced Energy Materials, College of Materials Science and Engineering, Sichuan University, Chengdu* 610064, *China*)

Abstract: Effects of high-energy ball milling on the microstructures of Si powders and consequently on the efficiency of Si-water reaction and the hydrogen generation behaviors are studied. During the milling process, both particle sizes and crystallite sizes of the powders decrease, but agglomerations, as well as the content of oxygen, internal strains, distortions and dislocations in the powders increase, and amorphous phase transformation of Si also appears on the particle surface. The increasing defects, including grain boundaries, internal strains, distortions and dislocations, amorphous phase transformation and powder refinement contribute to the hydrolysis performance of the powders. However, the growing contamination and agglomerations deteriorate the hydrolysis performance of the Si powders. The Si powders milled for 1 h have the best hydrolysis performances and produce 1 484.2 mL·g^{-1}_{Si} at 70 ℃, whose hydrogen conversion rate reaches 94%. However, the residual ~6%(*w*/*w*) of Si is out of reaction primarily owing to the fact that the hydrolysis byproduct SiO_2 adhering on the Si surface restrains the further reaction.

Keywords: hydrogen production; hydrolysis; powder refinement; silicon-water reaction

收稿日期:2018-03-14。收修改稿日期:2018-04-27。
*通信联系人。E-mail:wmeimeiw07@163.com

0 Introduction

As an energy carrier, hydrogen, with the characteristics of high energy density (142 $MJ \cdot kg^{-1}$, about three times higher than that of oil[1-2]) and zero emission, can be one of the best candidate fuels for fuel cell applications, such as domestic appliances and automobiles[3-4]. At present, the widely used on-site and on-demand hydrogen source technologies include compressed gaseous hydrogen storage and cryogenic liquid hydrogen storage. However, with high transportation cost and low safety[5], which impede their practical applications, they cannot meet all the requirements for light-duty vehicles issued by the US Department of Energy.

A variety of convenient chemical reactions to generate hydrogen on demand have therefore been examined[6-7], specially hydrolysis reactions of some cheap active metals and their hydrides, such as Al[8-9], Mg[10-11] and Mg-Ca alloy hydrides[12-13]. Compared with the traditional and reversible hydrogen storage, hydrolysis is an efficient and convenient hydrogen generation method, yielding pure hydrogen in much higher yield[14]. In recent years, silicon and silicon-based materials as hydrogen energy carrier have been investigated[15-20]. The reaction of silicon with water is shown as follows:

$$Si(s)+2H_2O(l) \rightarrow SiO_2(s)+2H_2(g) \quad (1)$$

This reaction is highly exothermic with a standard reaction enthalpy of $-409\ kJ \cdot mol^{-1}$ (298 K)[21]. To be a practical source of hydrogen, it is extremely favorable that the reaction can start off at room temperature without an external power supply. And the hydrolysis byproduct SiO_2 is easy to be recycled and reused for glass and cement[15]. It is known that silicon has advantages over aluminum and magnesium in terms of H_2 yield. Si shows higher gravimetric energy density, and one gram of Si produces 0.14 g of H_2, while the same mass of Al generates 0.11 g of H_2 and Mg generates 0.08 g of H_2. Besides, Si is the second most abundant element next to oxygen in the accessible Earth′s crust and available with a low cost[22]. Meanwhile, in strong contrast to oil and particular hydrogen, the transport and storage of silicon are free from potential hazards and require a simple infrastructure similar to that needed for coal[23]. Hence, silicon, abundant in earth, environmentally friendly, convenient for handling, has low density, high capacity and good activity in hydrolysis process, and is a promising material for on-board hydrogen generation, specially for portable power applications that use proton exchange membrane (PEM) fuel cells.

However, Si scarcely reacts with water under ambient conditions because a passive layer of silica forms at the silicon-water interface, which hinders the further reaction. To solve this problem, nanoporous Si powders formed by stain etching are prepared to maximize the surface area available for the reaction[16], and highly concentrated alkaline solution has also been applied to remove the oxide layer[17-18]. Other methods such as hydrogenating silicon[19] and compositing silicon with alloy elements[20] have also been studied. However, in spite of the progresses, a simplified and practical route to hydrogen generation by silicon has not been demonstrated. Al-based[24-26] or Mg-based materials[27-29] milled with or without additives have been considered as alternatives to generate hydrogen. The length of milling time is the most important parameter during the milling process. Shorter milling time does not attribute to particle refinement. But extended milling after a critical time leads to a decrease of a hydrogen yield due to the agglomerations and contaminations of the powders[30-32] or the formation of a secondary phase[33]. The microstructures, especially crystal defects of the materials change during the ball milling have effects on the hydrogen generation behaviors.

In this paper, structural evolution of the Si powders during high-energy ball milling and the hydrogen generation behaviors of the powders milled for different times are studied. Relationship between the microstructure characteristics and the hydrogen generation properties of the powders is also investigated to improve the hydrogen generation performances of the Si powders by ball milling.

1 Experimental

1.1 Sample preparation

The Si powders (~200 mesh) and KOH (AR, 99.9% purity) were purchased from Sigma-Aldrich company. The element analysis of the raw Si powders was tested by XRF (AXIOS 4Be-92U). The result is presented in Table 1. All materials were stored in an argon glove box with $<10^{-6}$ (V/V) H_2O and $<10^{-6}$ (V/V) O_2. The powders were introduced in a stainless-steel vial sealed under argon atmosphere and containing steel balls with a ball-to-powder (w_{ball}/w_{powder}=10). And the ball milling experiments were carried out in a SPEX 8000 high-energy ball mixer. The Si powders milled for 1 h were annealed at 600 ℃ for 12 h in a vacuum of 3 Pa, and then cooled down to room temperature in the furnace.

Table 1　XRF result of the raw Si powders

Element	Content / % (w/w)
Si	98.5
Fe	0.8
Al	0.5
Ca	0.2

1.2 Hydrolysis measurement

In each experiment, the hydrolysis reaction of (200±2) mg Si powders with 10 mL 0.5% (w/w) KOH aqueous solution occurred in a 250 mL round-bottom flask sealed by a dual-port tube with one for water inlet and the other for hydrogen output. The small amount of KOH served to dissolve any oxide formed on the Si surface in the form of soluble silicates to promote the hydrolysis of the powders[34]. Reaction temperature was controlled by a thermostatic water bath and the reactants were stirred during the reaction. The generated hydrogen flowed through a condenser at room temperature to be cooled down and through a dry tube filled with $CaCl_2$ to be dried. Then, it was measured by the water drainage method and collected in an inverted graduated cylinder filled with water. Each test was repeated at least twice to confirm the reliability. The hydrogen conversion yield (%) was equal to the ratio of the actual hydrogen yield to the theoretical hydrogen yield (1 576 $mL \cdot g^{-1}_{Si}$), assuming that the hydrogen was completely released as equation (**1**) and the solution is excluded in the calculation.

1.3 Structure and morphology characterization

The microstructure was analyzed by SEM (JEOL JSM-7500F, U=15 kV) and TEM (Zeiss Libra 200, U=200 kV). The element analysis was tested by EDS (GENESIS 2000 XMS). The particle sizes were measured using Laser Granulometry (Mastersizer 2000S) and the powders were deagglomerated in ethyl alcohol (AR, 99.9%) prior to the measurement, and D_{50} is presented as the particle size. The oxygen contents of different powders were measured by nitrogen\oxygen analyzer (NOA, LECO ON-736, USA). The phases and microstructure of the powders were analyzed by powder X-ray diffraction (XRD, DX-2700B equipment with Cu $K\alpha$ radiation with scanning speed of $0.04° \cdot s^{-1}$, λ= 0.154 18 nm, U=35 kV, I=25 mA, scanning angle from 10°~80°). The TG test was conducted by ZCT-A thermo gravimetric analyser (Beijing Jingyi High-tech Instrument Co., Ltd.), and argon was served as a protective gas. The samples were measured from 50 to 250 ℃ with a heating rate of 10 $℃ \cdot min^{-1}$.

2 Result and discussion

2.1 Effect of ball milling on microstructures

SEM images of the Si powders as illustrated in Fig.1 show typical micrographs of the powders milled for different times. A decrease in the particle sizes from about 40 μm for the umilled powders to 0.5 μm for the 2-hour milled is observed. The unmilled Si powders consist of irregular particles with the particle size distribution varying from a few micrometers to several dozens of micrometers (Fig.1(a)). After being milled for 0.5 h, large particles are rapidly pulverized to a few micrometers, and some small particles adhere to the surface of the large particles (Fig.1(b)). When the big particles are milled for 1 h, they continue to be fractured to small ones, which become agglomerated (Fig.1(c)). Subsequently, further milling makes the powders flat, agglomerated seriously (Fig.1(d)). Comparing the two insets of partial enlargement as seen in Fig.1(c,d), the powders milled for 2 h are agglomerated

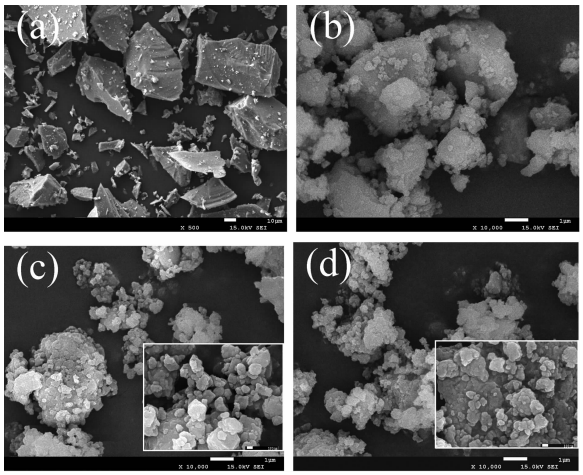

Fig.1 SEM images of (a) the unmilled Si powders and the Si powders milled for (b) 0.5, (c) 1 and (d) 2 h

more seriously than those milled for 1 h, but the particle size of the former seems nearly as small as the latter.

Fig.2 shows a great influence of ball milling time on the particle sizes of the Si powders. The ball milling time up to 1 h leads to an apparent decrease in the particle sizes. This result is identified by SEM images (Fig.1), showing that high-energy ball milling helps to decrease the particle sizes of the Si powders and subsequently refine them. But further milling up to 2 h only contributes to a slight further decrease of the particle sizes.

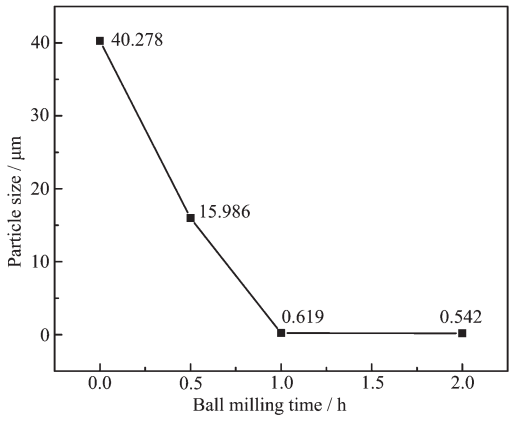

Fig.2 Particle sizes of the Si powders as a function of the milling time

Nonetheless, it is important to note that after stabilization of the particle sizes, microstructural refinement still takes place. In order to further investigate the phenomenon, the crystal structures of the Si powders after ball milling were analyzed. Fig.3 shows the X-ray diffraction patterns of the powders after different milling times. The positions of the diffraction peaks remain unchanged, indicating that the lattice parameters of the powders keep constant even after ball milling. However, representative (111), (220) and (311) planes (corresponding to 2θ=28.4°, 47.3° and 56.1°, respectively), which characterize crystalline silicon in the cubic structure, are gradually broadened with the milling time elongated. At the same time, intensities of the diffraction peaks are obviously weakened after milling, indicating a possible introduction of internal micro-strains inside and particle refinement of the Si powders, which lead to a decrease of Si crystallization. In addition, the XRD peaks of the powders milled for 1 h after heat treatment become narrower and sharper, indicating a more integral crystal lattice.

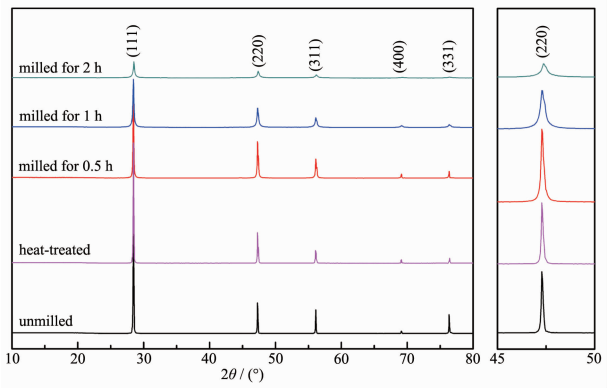

Fig.3 X-ray diffraction patterns of the Si with different milling times and the powders milled for 1 h after heat treatment

A Rietveld refinement analysis of the Si powders milled for different times was performed to determine the Si crystallite sizes and the internal strains, and the results are presented in Fig.4 and Table 2. The crystallite size reduces to 48.2 nm after being milled for 1 h and tends to be stable with further milling. That is to say, the ball milling contributes to refinement of the crystal grains in a way. However, the smaller the crystallite sizes, the more the grain boundaries. The decrease of the crystallite sizes is also accompanied by the increase of the internal strains after ball milling. The internal strains (ε) in the powders milled

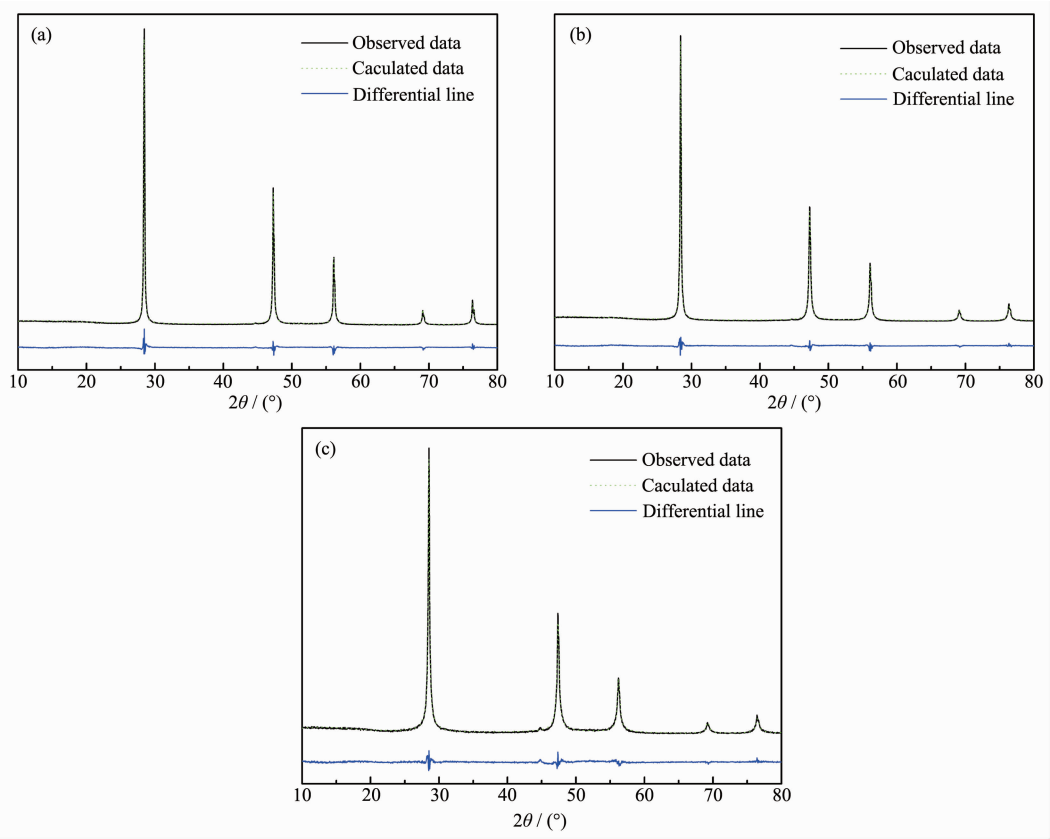

Fig.4　XRD Rietveld refinement patterns of the Si powders milled for (a) 0.5, (b) 1 and (c) 2 h

Table 2　Rietveld refinement results of the Si powders with different milling times

Materials	Unmilled*	Milled for 0.5 h	Milled for 1 h	Milled for 2 h
Crystallite size / nm	—	>100	48.2	43.1
Internal strains / %	—	0.141	0.204	0.395
R_{wp} / %	—	7.77	6.96	9.82

*: R_{wp} (weighted pattern coefficient of determination) of the umilled Si powders is too high and the result is not shown.

for 2 h (ε=0.395%) is much higher than those in the powders milled for 0.5 h (ε=0.141%). The results are consistent with XRD patterns (Fig.3). The ball milling time up to 1 h leads to an apparent decrease in the grain sizes, which causes the intensity reduction of the diffraction peaks. Further milling up to 2 h contributes to a slight decrease of the grain sizes and an obvious increase of the internal strains, which are responsible for the intensity reduction of the diffraction peaks of the Si powders milled for 2 h.

To represent the microstructures of the Si powders directly, TEM investigation was carried out employing imaging and diffraction modes. Fig.5 shows the TEM images of the Si powders milled for different times. Fig.5(a) shows high-resolution (HR) TEM image and Fourier function transformation (FFT) image of the powders milled for 0.5 h. Only crystalline regions are found and the crystal plane spacing of the crystalline structure is 0.315 nm, which is consistent with the (111) plane of Si. Fig.5(b) is the inversed FFT image from filtered FFT in Fig.5(a). Edge-like dislocations and lattice distortions are indicated by dotted circles and ellipses respectively in Fig.5(b). As shown in the figure, some lattice distortions and dislocations exist and the edge dislocations are exhibited with the burgers vector perpendicular to (111) planes. Fig.5(c) shows the HRTEM image and the FFT image of the powders milled for 1 h. Both crystalline regions and amorphous regions are exhibited as labeled in Fig.5(c). The amorphous regions are mainly distributed in the

near surface area of the powders, which is not found in those milled for 0.5 h. And the crystal region locates inside of the particle, whose crystal plane spacing is 0.315 nm and consistent with the (111) plane. Seen from Fig.5(d), the inversed FFT image from filtered FFT of Fig.5(c), the lattice defects are also found in the powders and the number of distortions and dislocations of the powders milled for 1 h is much higher than that of the powders milled for 0.5 h (Fig.5 (b)). According to the TEM images, it is obvious that the elongated ball milling time makes crystalline silicon to transform into partial amorphous phase and increases the lattice defects.

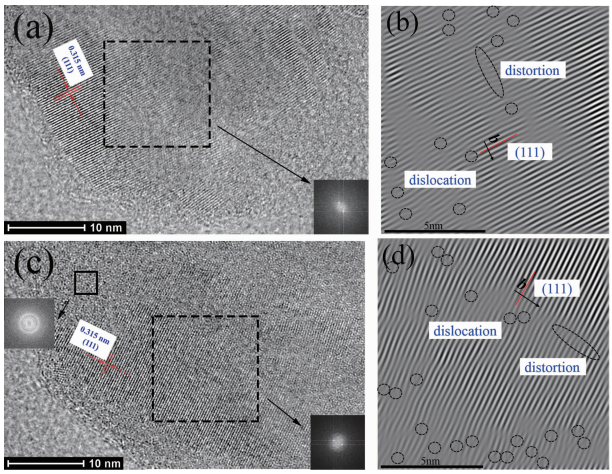

Fig.5 High-resolution (HR) TEM images and the Fourier function transformation (FFT) images of the Si powders milled for (a) 0.5 and (c) 1 h; (b) and (d) inversed FFT images from filtered FFT of dotted boxes in (a) and (c), respectively

The long-time milling possibly leads to contamination by iron and/or oxygen to the powders. An iron concentration in the Si powders is less than 0.1% (*w*/*w*). Fe reacts little with H_2O during the hydrolysis of Si and even slows the reaction rate when the Fe_xSi_y phase exists in the powders[35]. Because the content is very small, the effect is ignored in this work. The nitrogen/oxygen analyzer is applied to examine the oxygen contents in the powders. The increase of the oxygen content in the powders with the increasing milling time is confirmed in Fig.6. An oxygen concentration of 1.986% (*w*/*w*) is measured for the powders milled for 2 h contrasted to 0.120 1% (*w*/*w*) for the unmilled. However, the result of XRD does not show any silicon oxide phase in the powders. Assuming that all oxygen is in SiO_2, it corresponds to a SiO_2 content of 3.72% (*w*/*w*) (2-h milled) and 0.225% (*w*/*w*) (unmilled), respectively. Thus, on the basis of the O contamination measurements, no silicon oxide phase is observed in the XRD patterns, because its diffraction peaks are so weak that they are concealed in the strong diffraction peaks of the Si powders.

2.2 Effect of ball milling on hydrogen generation properties

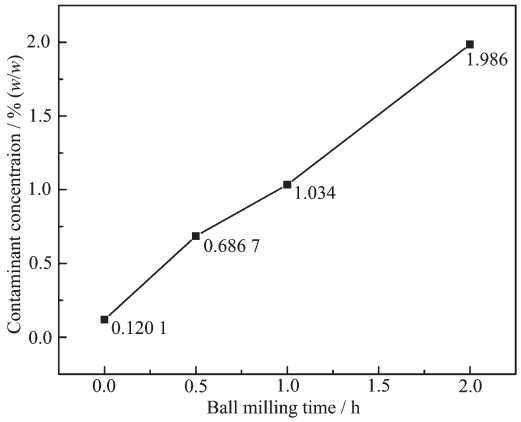

Fig.6 Concentration of contaminant (O) in the Si powders as a function of the milling time

In order to investigate the effect of milling conditions on the hydrolysis properties of the Si powders, the powders with different milling times were introduced into KOH aqueous solution to react with water, as shown in equation (**1**). Fig.7 shows hydrogen generation curves of the powders milled for different times in 0.5% (*w*/*w*) KOH solution at 25 ℃. The hydrolysis rate and the hydrogen yield of the Si powders increase with the elongation of the milling time, and the hydrolysis efficiency reaches the maximum after the powders being milled for 1 h, then the hydrolysis rate and the hydrogen generation of the powders decrease after being milled for over 1 h. Indeed, the unmilled powders have very low reactivity and react slowly in the solution to generate hydrogen, and the maximum conversion yield reaches only 13% after 90 min of reaction. However, the powders milled for 1 h have the highest hydrogen yield of 69% during the hydrolysis for 90 min. Furthermore, the unmilled

powders and the powders milled for 0.5 and 1 h produce 197.9, 766.8 and 1 085.6 mL·g$^{-1}_{Si}$ in 90 min respectively, which indicates that the first 0.5 h of milling has greater influence on the hydrolysis properties of the Si powders than the second 0.5 h of milling time. At the same time, the hydrolysis rate and the hydrogen yield of the Si powders milled for 1 h after heat treatment slightly decrease compared with those of the powders before heat treatment, however, they are still much greater than those of the powders milled for 0.5 h.

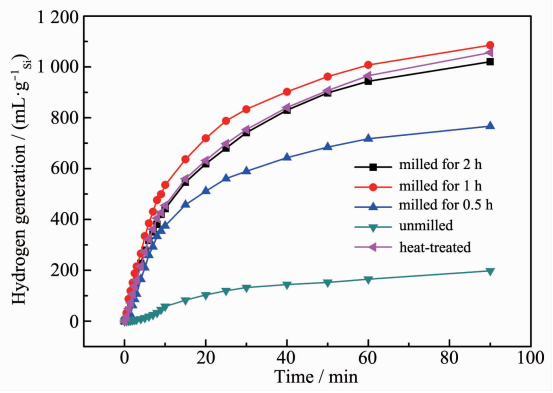

Fig.7　Hydrogen generation curves of the Si powders with different milling times and the powders milled for 1 h after heat treatment in KOH solution at 25 ℃

Fig.8 shows the average hydrogen generation rate within different periods of the Si powders as a function of the milling times. The unmilled powders only produce 57.7 mL·g$^{-1}_{Si}$ in 10 min and those milled for 0.5, 1 and 2 h produce 375.2, 535.9 and 442.2 mL·g$^{-1}_{Si}$, respectively, which indicates that the first 1 h of milling contributes mostly to the initial hydrogen generation rate of the powders. After hydrolysis for 10 min, the hydrogen generation rate of the powders declines quickly, but the powders milled produce

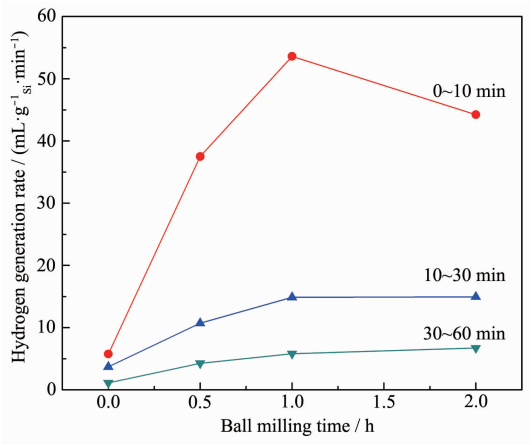

Fig.8　Average hydrogen generation rate within different periods of the Si powders with different milling times

hydrogen continuously. Generally speaking, the ball milling promotes the hydrolysis performances of the powders.

It can be concluded that appropriate time of milling can indeed improve the hydrolysis properties of the Si powders at 25 ℃. However, the overall hydrogen yields are still under anticipation, indicating that milling is effective but the effects are probably limited at room temperature. To reveal that, the powders with different milling times at different hydrolysis temperatures were analyzed. Fig.9 shows the hydrogen generation curves of the Si powders milled for different times in KOH solution at different temperatures. From Fig.9, it is clearly seen that a temperature growing of the solution promotes the hydrogen generation. In the solution at 25, 40, 55 and 70 ℃, the powders milled for 1 h produce 1 085.6, 1 282.6, 1 420.0 and 1 484.2 mL·g$^{-1}_{Si}$ in 90 min, respectively. Accordingly, the maximum conversion yield of the powders milled for 1 h reaches 68%, 81%, 90% and 94%, respectively. In

Table 3　Hydrolysis properties of the Si powders with different milling times

Materials		Temperature / ℃				Theoretical H_2 yield / (mL·g$^{-1}_{Si}$)
		25	40	55	70	
unmilled	H_2 yield / (mL·g$^{-1}_{Si}$)	197.9	346.3	432.9	589.5	1 576
	H_2 conversion yield / %	13	22	27	37	
milled for 0.5 h	H_2 yield / (mL·g$^{-1}_{Si}$)	766.8	938.7	1 108.3	1 294.5	
	H_2 conversion yield / %	49	60	70	82	
milled for 1 h	H_2 yield / (mL·g$^{-1}_{Si}$)	1 085.6	1 282.6	1 420.0	1 484.2	
	H_2 conversion yield / %	69	81	90	94	

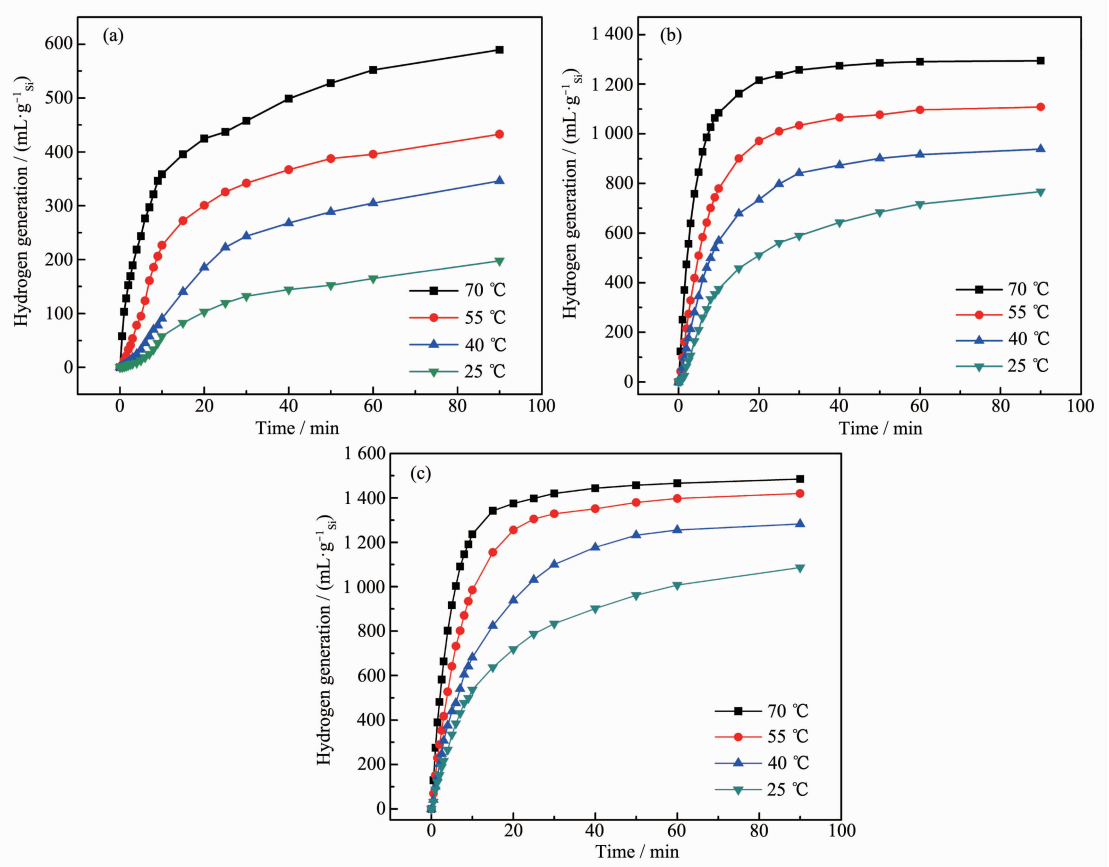

Fig.9 Hydrogen generation curves of (a) the unmilled Si powders and the Si powders milled for (b) 0. 5 and (c) 1 h

addition, the hydrolysis properties of the unmilled powders and the powders milled for 0.5 h as counterparts are also investigated, and their hydrolysis performances are listed in Table 3. As shown in Fig.8 and Table 3, the hydrolysis reactions of all Si powders are affected by temperature significantly. The higher the temperature, the faster the hydrogen evolution rate and the higher the hydrogen yield.

2.3 Relationship between microstructures and hydrogen generation properties

Based on the morphology analysis of the Si powders mentioned in chapter 2.1, the increase of milling time leads to a decrease of the particle sizes of the powders to some degree. The morphological changes during ball milling of the powders can be explained by assuming that there is a competition between two mechanisms: the fracture and the agglomeration. And when a balance is maintained between the cold welding and the fracture of the particles, the particle size of the powders is constant[36]. During the first 1 h of milling, the Si particles tend to be fractured to small ones due to high brittlement, and the particle size decreases obviously (Fig.1(a,b) and Fig.2). When the particles are small enough with high specific surface area and have many new surfaces, they tend to be agglomerated (Fig.1(c,d)). So, during the prolonged milling process, there is a constant interplay between the cold welding and the fracture of the Si particles, and the size of the particles keeps steady (Fig.2).

At the same time, when the particles are less than 0.619 μm, they tend to be contaminated more easily (Fig.2 and Fig.6). And the longer the milling time, the more easily the powders are contaminated. Therefore, the oxygen content in the powders increases with growing milling time (Fig.6).

During the high-energy ball milling, whenever two steel balls collide, some amounts of powders are trapped in between them. The impact force is great and makes the particles deform, leading to defects

formation in the grains. Hence, from the results of XRD Rietveld refinement results and TEM images, the amounts of defects increase with the prolonged milling time. When dislocations are accumulated, they are polygonized to form subgrain boundaries firstly, and then they are evolved to high-angle grain boundaries, which refines the grains consequently [37]. Thus the crystallite sizes of the Si powders decrease gradually during the milling process as seen in Table 2. Consequently, the small crystallite sizes and high internal strains make the crystalline structure unstable and induce the crystalline silicon to transform into the amorphous phase [38] (Fig.5). However, the crystallite sizes decrease slowly after a long time milling perhaps due to the greater Si-Si bond within the small grains than that on the grain boundaries.

Because the milling time has great influence on the microstructures of the Si powders, the hydrogen generation performances of the powders milled for different times by reacting with water also differ from each other. As previously demonstrated, the ball milling helps to refine the powders. Powder refinement is correlated with specific area increment, which means an adequate contact between the particles and water.

Meanwhile, the high-energy ball milling leads to amorphous phase transformation and increasing the lattice defects including the grain boundaries, the internal strains, distortions and dislocations. The Si atoms near the defects are unstable, and have high energy and activity. And they react with water easily, improving their hydrolysis performances like Al-based or Mg-based materials[28]. Besides, heat treatment makes the Si powders exhibit a more integral crystal lattice. A little difference between the hydrolysis performances of the Si powders before and after heat treatment approves that amorphous phase transformation slightly contributes to the hydrolysis performance of the powders. But the hydrolysis performance of the Si powders milled for 1 h after heat treatment is still much better than that of the powders milled for 0.5 h without heat treatment, which indicates that the effect of powder refinement on the hydrolysis performance is greater than that of the amorphous phase transformation.

However, for the milled Si powders, the above result seems not reasonable, because that after being milled for 1 h, the sizes of the particles continue to decrease, but the hydrolysis rate and hydrogen generation of the powders decrease on the contrary. As seen in Fig.1(c,d) and Fig.2, the powders milled for 2 h are agglomerated more seriously and have higher oxygen content than those milled for 1 h. These factors doom to worsen the hydrogen generation performances of the powders.

SEM micrograph and EDS pattern of insoluble residue after the hydrolysis of the Si powders in KOH aqueous solution at room temperature are shown in Fig.10. The SiO_2 particles are agglomerated seriously, and adhere on the surface of the Si particles (Fig.10(a)).

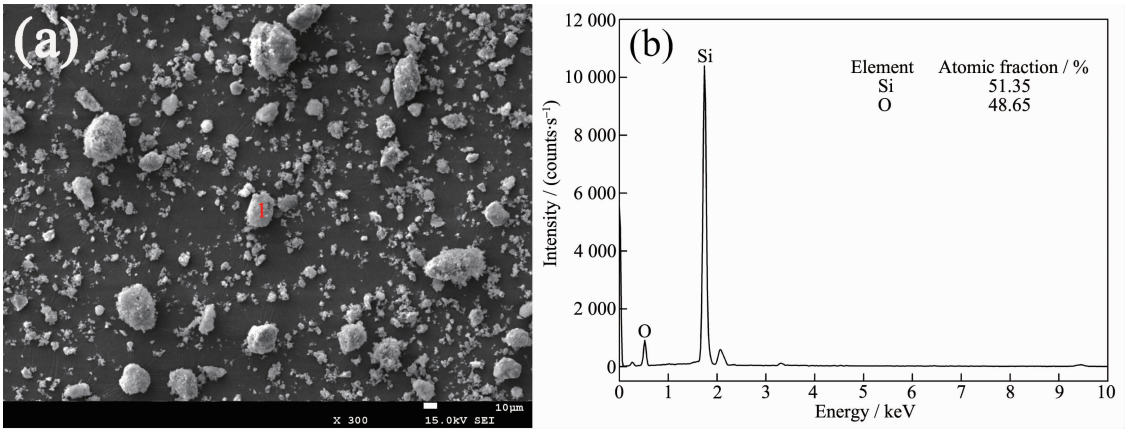

Fig.10　(a) SEM micrograph of the insoluble residue after the Si powders hydrolysis in KOH aqueous solution at room temperature and (b) EDS pattern of the position 1 in the SEM micrograph

The refined SiO_2 adhering on the surface of Si particles continue to grow up and then a passive layer is formed, which overwraps the unreacted Si particles and leads to the cease of hydrolysis. This explains why the conversion yield of the powders does not reach 100%. In order to demonstrate the inexistence of hydrated silica, TG test is conducted on the insoluble residue, as shown in Fig.11. The samples have a little weight increase, which verifies the inexistence of hydrated silica. And the weight increases may be caused by the oxidization of the unreacted Si during the heating process in the TG test.

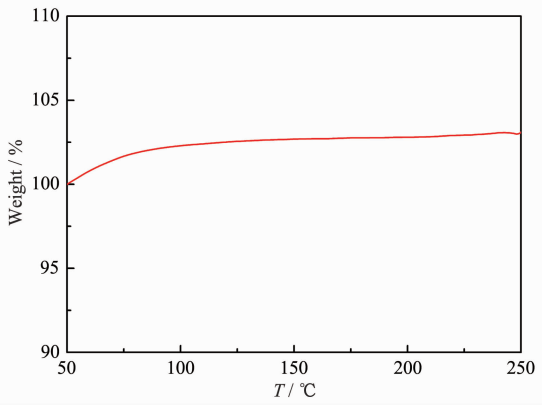

Fig.11 TG curves of the insoluble residue after the Si powders hydrolysis in KOH aqueous solution at room temperature

Temperature rising of the solution promotes the hydrogen generation performances of the Si powders milled for different time. The role of KOH makes a conversion of SiO_2 to soluble silicates[39], thus exposing internal unreacted silicon to water:

$$SiO_2(s)+2OH^-(aq) \rightarrow H_2SiO_4^{2-}(aq) \quad (2)$$

The by-product $H_2SiO_4^{2-}$ may partly hydrolyze further and provide some OH^- for equation (**2**), which promotes equation (**1**) as follows:

$$H_2SiO_4^{2-}(aq)+H_2O(l) \rightarrow H_3SiO_4^-(aq)+OH^-(aq) \quad (3)$$

Because equation (**3**) is endothermic and is accelerated by the temperature growing, the hydrogen evolution rate and the hydrogen yield of the powders improve with the elevated hydrolysis temperature. When the temperature is elevated, the high chemical reactivity of Si and the high dissolubility of the by-product also promote the hydrogen generation process.

Meanwhile, the hydrolysis performance of Si is possibly influenced by the impurity elements in the raw Si powders (Table 1). There are some previous reports about the effects of these elements. Fe only reacts little with H_2O and slows the reaction rate when the Fe_xSi_y phase exists in the powders[35]. The hydrolysis reactivity of Al is higher than that of Si in the alkaline solution[40]. And Ca in the Si powders promotes the hydrogen generation like Mg-based [12] and Al-based[41] materials. Because the contents of these impurity elements are very small, the effects are ignored and not discussed in this work.

High-energy ball milling promotes the hydrogen generation process of the Si powders to some degree. But it is necessary to optimize the milling time for a higher hydrogen yield and lower energy consumption. To dispel the above-mentioned adverse factors and take full advantage of milling, the Si powders milled in H_2 atmosphere, or with benzene or cyclohexane as additives is under consideration.

3 Conclusions

In this work, the relationship between microstructures and the hydrolysis performances of the ball-milled Si powders was investigated. High-energy ball milling helps to refine the powders, make the powders amorphous partially and increase their lattice defects including the grain boundaries, the internal strains, distortions and dislocations. These factors contribute to the hydrolysis performance of the powders. On the other hand, a longer time of ball milling causes the powders to be contaminated and agglomerated, which deteriorates the hydrolysis performance of the powders. Above all, the powders milled for 1 h have the best hydrogen generation performance, and produce 1 085.6 $mL \cdot g^{-1}_{Si}$ at 25 ℃. At 70 ℃, the hydrogen conversion rate of the powders milled for 1 h reaches 94% and hydrogen generation rate is 16 $mL \cdot g^{-1}_{Si} \cdot min^{-1}$. The residual ~6% of Si is out of reaction primarily owing to the fact that the hydrolysis byproduct SiO_2 adhering on the Si surface restrains the further reaction.

References:

[1] Muir S S, Yao X. *Int. J. Hydrogen Energy*, **2011**,**36**:5983-5997

[2] Jain I P, Lal C, Jain A. *Int. J. Hydrogen Energy*, **2010**,**35**:5133-5144

[3] Hardman S, Chandan A, Steinberger-Wilckens R. *J. Power Sources*, **2015**,**287**:297-306

[4] Zhang X, Chan S H, Ho H K, et al. *Int. J. Hydrogen Energy*, **2015**,**40**:6866-6919

[5] Tayeh T, Awad A S, Nakhl M, et al. *Int. J. Hydrogen Energy*, **2014**,**39**:3109-3117

[6] Xu Y M, Wu C L, Chen Y G, et al. *J. Power Sources*, **2014**, **261**:7-13

[7] Liu Y G, Wang X H, Liu H Z, et al. *J. Energy*, **2014**,**68**:548-554

[8] Dai H B, Ma G L, Xia H J, et al. *Energy Environ. Sci.*, **2011**,**4**:2206-2212

[9] Chen Y K, Teng H T, Lee T Y, et al. *Int. J. Energ. Environ. Eng.*, **2014**,**5**:1-6

[10]Si T Z, Han L, Li Y T, et al. *Int. J. Hydrogen Energy*, **2014**, **39**:11867-11872

[11]Tegel M, Schne S, Kieback B, et al. *Int. J. Hydrogen Energy*, **2017**,**42**:2167-2176

[12]Liu P P, Wu H W, Wu C L, et al. *Int. J. Hydrogen Energy*, **2015**,**40**:3806-3812

[13]Li J F, Liu P P, Wu C L, et al. *Int. J. Hydrogen Energy*, **2016**,**42**:1429-1435

[14]Demirci U B, Akdim O, Miele P. *Int. J. Hydrogen Energy*, **2009**,**34**(6):2638-2645

[15]Auner N. *General Information*, **2004**,**44**(Supplement s6):59-63

[16]Litvinenko S, Alekseev S, Lysenko V, et al. *Int. J. Hydrogen Energy*, **2010**,**35**:6773-6778

[17]Goller B, Kovalev D, Sreseli O. *Nanotechnology*, **2011**,**22**:305-402

[18]Erogbogbo F, Lin T, Tucciarone P M, et al. *Nano Lett.*, **2013**,**13**:451-456

[19]Kale P, Gangal A C, Edla R, et al. *Int. J. Hydrogen Energy*, **2012**,**37**:3741-3747

[20]Zhan C Y, Chu P K, Ren D, et al. *Int. J. Hydrogen Energy*, **2011**,**36**:4513-4517

[21]Weast R C. *CRC Handbook of Chemistry and Physics*. 1*st Student Ed*. Boca Raton: CRC Press, **1988**:69

[22]Earnshaw A, Greenwood N. *Chemistry of the Elements*. 2*nd Ed*. Oxford: Butterworth-Heinemann, **1997**:122

[23]Auner N, Holl S. *Energy*, **2006**,**31**:1395-1402

[24]Ilyukhina A V, Kravchenko O V, Bulychev B M, et al. *Int. J. Hydrogen Energy*, **2010**,**35**:1905-1910

[25]Fan M Q, Sun L X, Xu F. *Energy Convers. Manage*., **2010**, **51**:594-599

[26]Fan M Q, Sun L X, Xu F. *Energy*, **2010**,**35**:1333-1337

[27]Ouyang L Z, Huang J M, Wang H, et al. *Int. J. Hydrogen Energy*, **2013**,**38**:2973-2978

[28]Huang M H, Ouyang L Z, Ye J S, et al. *J. Mater. Chem. A*, **2017**,**5**:8566-8575

[29]Wang C P, Yang T, Liu Y H, et al. *Int. J. Hydrogen Energy*, **2014**,**39**:10843-10852

[30]Grosjean M H, Zidoune M, Roué L, et al. *Int. J. Hydrogen Energy*, **2006**,**31**:109-119

[31]Fan M Q, Xu F, Sun L X. *Int. J. Hydrogen Energy*, **2007**, **32**:2809-2815

[32]Razavi-Tousi S S, Szpunar J A. *Int. J. Hydrogen Energy*, **2013**,**38**:795-806

[33]Wang H W, Chung H W, Teng H T, et al. *Int. J. Hydrogen Energy*, **2011**,**36**:15136-15144

[34]Xu L, Ashraf S, Hu J P, et al. *Int. J. Hydrogen Energy*, **2016**,**41**:12730-112737

[35]Brack P, Dann S E, Wijayantha K G U, et al. *Int. J. Energy Res.*, **2017**,**41**(12):1740-1748

[36]Suryanarayana C. *Prog. Mater. Sci.*, **2001**,**46**:11-39

[37]XIAO Jun(肖军), PAN Jing(潘晶), LIU Xing-Cai(刘新才). *Magnetic Materials and Devices*(磁性材料与器件), **2005**, **36**:6-7

[38]Gaffet E, Harmelin M. *J. Less-Common Met.*, **1990**,**157**:201-222

[39]Stephen R G, Riley F L. *J. Eur. Ceram. Soc*., **1989**,**5**:219-222

[40]Yoo H S, Ryu H Y, Cho S S, et al. *Int. J. Hydrogen Energy*, **2011**,**36**(23):15111-15118

[41]Zhao Z W, Chen X Y, Hao M M. *Energy*, **2011**,**36**:2782-2787